NMR Assignment of *Rhodobacter capsulatus* Ferricytochrome c′, a 28 kDa Paramagnetic Heme Protein†

Michael Caffrey,‡ Jean-Pierre Simorre,‡ Bernhard Brutscher,‡ Michael Cusanovich,§ and Dominique Marion*,‡

Institut de Biologie Structurale Jean-Pierre Ebel, CNRS-CEA, 41, avenue des Martyrs, 38027 Grenoble Cedex, France, and Department of Biochemistry, University of Arizona, Tucson, Arizona 85721

Received December 19, 1994; Revised Manuscript Received February 27, 1995⊗

ABSTRACT: The cytochromes *c′* are paramagnetic heme proteins generally consisting of two identical 14 kDa subunits. The ^{1}H and ^{15}N resonances of the ferricytochrome *c′* from the purple phototrophic bacterium *Rhodobacter capsulatus* have been extensively assigned by the TOCSY-HSQC, NOESY-HSQC, HSQC-NOESY-HSQC, and HNHA 3D heteronuclear experiments performed on an 8 mM sample labeled with ^{15}N. In addition, the $^{13}C^{\alpha}$ and ^{13}CO resonances were assigned by the HNCA and multiple-quantum HNCOCA 3D experiments performed on a 0.5 mM sample labeled with ^{13}C and ^{15}N. The assignment of the backbone ^{13}C resonances was used to confirm the ^{1}H and ^{15}N assignments and to better define secondary structure. On the basis of medium-range NOEs, $^{3}J_{HN\alpha}$ coupling constants, and backbone ^{13}C chemical shifts, the secondary structure consists of four helices: helix-1 (3−29), helix-2 (33−49), helix-3 (78−97), and helix-4 (103−117). On the basis of long-range NOE contacts, the *Rb. capsulatus* ferricytochrome *c′* is a four-helix bundle protein in which consecutive helices are antiparallel with respect to one another.

The cytochromes *c′* are paramagnetic heme proteins, which are found in the periplasmic space of phototrophic bacteria (Bartsch, 1978; Meyer & Kamen, 1982). Cytochromes *c′* are characterized by covalent attachment of the heme to a CXXCH motif which is located near the carboxy terminus *and* the absence of a sixth heme ligand. In general, they consist of two identical 14 kDa subunits resulting in a 28 kDa complex. The X-ray structures of the cytochromes *c′* from *Rhodospirillum molischianum* (Finzel et al., 1985), *Rhodospirillum rubrum* (Yasui et al., 1992), and *Chromatium vinosum* (Ren et al., 1993) reveal that the cytochromes *c′* possess a four-helix bundle structural motif. Interestingly, the four-helix bundle motif is also found in many non-heme proteins including apoferritin, interleukin 4, and tobacco mosaic virus coat protein (Presnell & Cohen, 1989). Although the *in vivo* function of the cytochromes *c′* is presently unknown, they are widely found among the photosynthetic bacteria, and their concentration levels appear to increase under photosynthetic growth conditions (Meyer & Kamen, 1982). Consequently, they are presumably involved in photosynthesis. The cytochromes *c′* exhibit a number of unusual properties. First, the heme is paramagnetic in both redox states. In the oxidized and reduced states, the heme iron is generally high spin with $S = {}^{5}/_{2}$ and $S = 2$ for the oxidized and reduced states, respectively (Moore & Pettigrew, 1990, and references therein), although the ferric irons of the *C. vinosum* and *Rhodobacter capsulatus* cytochromes *c′* are proposed to exist as quantum mechanically admixed spin states of $S = {}^{5}/_{2}$ and $S = {}^{3}/_{2}$ at neutral pH (Maltempo & Moss, 1976; La Mar et al., 1990; Monkara et al., 1992). Thus, the cytochromes *c′* are models for the electronic environment of heme proteins. Second, the cytochromes *c′* bind CO and NO as axial ligands of the heme iron. The cytochromes *c′* from species such as *Rsp. molischianum* and *Rb. capsulatus* bind CO and NO noncooperatively, in a manner similar to myoglobin (Cusanovich & Gibson, 1973; Doyle et al., 1985; Kassner, 1991; Caffrey and Cusanovich, unpublished results). In contrast, the cytochromes *c′* from species such as *C. vinosum* and *Rsp. rubrum* bind CO and NO cooperatively, in a manner analogous to the hemoglobins (Cusanovich & Gibson, 1973; Doyle et al., 1986, Kassner, 1991; Caffrey and Cusanovich, unpublished results). Indeed, in the case of *C. vinosum* cytochrome *c′*, binding of CO has been shown to result in conformational changes, which cause a dimer to monomer transition (Doyle et al., 1986). Consequently, the cytochromes *c′* serve as models for cooperative interactions in proteins.

The study of the cytochromes *c′* by NMR[1] is hampered by a number of difficulties. First, the cytochrome *c′* monomers consist of approximately 130 residues, which is near the limit for study by homonuclear NMR due to spectral overlap of the ^{1}H resonances. Second, the cytochromes *c′* are primarily helical proteins, and thus the assignment is complicated by inefficient coherence transfer in NMR experiments due to small $^{3}J_{HN\alpha}$ values and poor dispersion of H^{α} chemical shifts. Third, the complex molecular mass is 28 kDa, and hence all nuclei will exhibit relatively fast transverse relaxation rates (i.e., short T_2 times) due to slow molecular tumbling, with respect to smaller molecular weight complexes. The increased relaxation rates lead to line-broadening of signals and thus lower signal to noise ratios and increased spectral overlap. Finally, the heme iron is paramagnetic in both redox states. Consequently, all nuclei

† Financial support was provided in part by NIH Grant GM21277.
* To whom correspondence should be addressed.
‡ CNRS-CEA.
§ University of Arizona.
⊗ Abstract published in *Advance ACS Abstracts,* April 15, 1995.

[1] Abbreviations: HMQC, heteronuclear multiple-quantum coherence spectroscopy; HSQC, heteronuclear single-quantum coherence spectroscopy; NMR, nuclear magnetic resonance; NOE, nuclear Overhauser effect; NOESY, nuclear Overhauser enhancement spectroscopy; ROE, rotating frame NOE; TOCSY, total correlated spectroscopy; TPPI, time-proportional phase incrementation; WATERGATE, water suppression by gradient-tailored excitation.

0006-2960/95/0434-5904$09.00/0

in close proximity to the heme iron will experience increased relaxation rates with a $1/r^6$ distance dependence, where r is the electron−nucleus distance (Swift, 1973). Nuclei with decreased T_2 will exhibit increased line widths and hence be more difficult to detect due to lower signal to noise ratios. Together, these factors have limited previous NMR studies of the cytochromes *c'* to the well-resolved protons of the heme group and neighboring residues (cf., La Mar et al., 1990; Banci et al., 1992).

In what follows, we present extensive assignments for the ^1H , ^{13}C, and ^{15}N resonances of *Rb. capsulatus* ferricytochrome *c'* by a combination of 3D heteronuclear experiments. We will show the utility of using a relatively concentrated sample labeled with ^{15}N in concert with a relatively dilute sample labeled with ^{13}C and ^{15}N. We demonstrate that many of the problems of spectral overlap are overcome by multidimensional heteronuclear experiments. Moreover, the decreased sensitivity of NOESY experiments, which results from the significant relaxation effects that are present in large paramagnetic proteins, can be overcome by a concentrated ^{15}N-labeled sample. We will show that medium-range NOEs, $^3J_{HN\alpha}$ coupling constants, and backbone ^{13}C chemical shifts are consistent with a four-helix bundle structural motif, which is most similar to those observed for the X-ray structures of *Rps. rubrum* and *C. vinosum* cytochromes *c'*. In addition, a topological model of the *Rb. capsulatus* ferricytochrome *c'* will be presented based on long-range NOE contacts. Finally, we will discuss the significance of the residues that could not be assigned.

MATERIALS AND METHODS

Protein Preparation. For the preparation of the ^{15}N-labeled sample, *Rb. capsulatus* strain MT-1141 was grown photosynthetically in 1-L bottles under saturating light conditions (Caffrey et al., 1992). Media conditions were as previously described (Weaver et al., 1975) except that $^{15}NH_4Cl$ was added as the sole nitrogen source to a concentration of 0.5 g/L. The $^{13}C/^{15}N$-labeled sample was prepared as previously described (Caffrey et al., 1994). Cytochrome *c'* was purified according to the method of Bartsch (1978) to a final A_{280}/A_{400} ratio of 0.25 in the oxidized state. For the NMR experiments, the ^{15}N-labeled sample was concentrated at room temperature to approximately 8 mM (heme concentration) in buffer containing 100 mM PO_4 (pH 6.0), 25 μM chloramphenicol (to inhibit bacterial growth), and 10% D_2O. The $^{13}C/^{15}N$-labeled sample was concentrated to a volume of approximately 200 μL and placed in a Shigemi NMR tube (Shigemi Inc., Allison Park, PA). The final concentration of the $^{13}C/^{15}N$-labeled sample was approximately 0.5 mM in buffer containing 100 mM PO_4 (pH 6.0), 50 μM sodium azide (to inhibit bacterial growth), and 10% D_2O. Oxygen was removed by blowing argon gas over the solution surface for approximately 15 min.

NMR Experiments. NMR experiments were performed on a Bruker AMX600 spectrometer equipped with either reverse ^1H-X broad-band or ^1H, ^{13}C, and ^{15}N triple-resonance probes operating at temperatures of 300 or 310 K. 2D TOCSY experiments (Davis & Bax, 1985) employed an isotropic mixing time of 40 ms (not including delays inserted to balance transverse and longitudinal NOE); the field strength of the ^1H WALTZ-16 spin lock was 12 kHz. 2D NOESY experiments employing a heteronuclear half-filter were as described by Otting and Wüthrich (1990) with NOE mixing times of 50 and 120 ms. For the 2D data sets, the spectral widths for the direct and indirect dimensions were 14 and 12 ppm, respectively. The carrier positions for ^1H and ^{15}N were 4.75 and 117.4 ppm, respectively. Spectra were acquired with 800 complex points in t_1 and 48 scans per t_1 increment for a total experimental time of 12 h. The 3D TOCSY-HSQC, NOESY-HSQC, and HSQC-NOESY-HSQC experiments were similar to the TOCSY-HMQC (Marion et al., 1989b), NOESY-HMQC (Kay et al., 1989), and HMQC-NOESY-HMQC (Ikura et al., 1990) experiments previously described except for the following modifications: (1) the HSQC sequence (Bodenhausen & Ruben, 1980) was used as opposed to the HMQC sequence to increase the resolution of the ^{15}N dimension; (2) pulsed field gradients (Bax & Pochapsky, 1992) were added to suppress undesired coherence transfer pathways. In addition, the WATERGATE sequence (Sklenàr et al., 1993) was added for solvent suppression in the TOCSY-HSQC and NOESY-HSQC experiments. For the TOCSY-HSQC and NOESY-HSQC experiments, the spectral widths for ^1H, ^{15}N, and ^1H were 7, 30, and 12 ppm, respectively; carrier positions for ^1H, ^{15}N, and ^1H were 8.40, 117.4, and 4.75 ppm, respectively. Spectra were acquired with 256 complex points in t_1, 80 complex points in t_2, and 8 scans per t_1/t_2 increment, resulting in a total experimental time of approximately 60 h. For the TOCSY-HSQC experiment, the isotropic mixing time was 40 ms (not including delays) and the field strength of the ^1H WALTZ-16 spin lock was 12 kHz. For the HSQC-NOESY-HSQC experiment, the spectral widths for ^{15}N, ^{15}N, and ^1H were 30, 30, and 7 ppm, respectively; carrier positions for ^{15}N, ^{15}N, and ^1H were 117.4, 117.4, and 8.40 ppm, respectively. Spectra were acquired with 92 complex points in t_1, 92 complex points in t_2, and 16 scans per t_1/t_2 increment, resulting in a total experimental time of approximately 60 h. For the NOESY-HSQC and HSQC-NOESY-HSQC experiments, the mixing time was 120 ms. The 3D HNHA experiment was identical to that of Vuister and Bax (1993). Spectral widths for ^{15}N, ^1H, and ^1H were 30, 11, and 7 ppm, respectively. Carrier positions for ^{15}N, ^1H, and ^1H were 117.4, 4.75, and 8.40 ppm, respectively. Spectra were acquired with 48 complex points in t_1, 76 complex points in t_2, and 48 scans per t_1/t_2 increment, resulting in a total experimental time of approximately 60 h. The 3D HNCA experiment was performed as previously described (Grzesiek & Bax, 1992). Spectral widths for ^{15}N, ^{13}C, and ^1H were 30, 30, and 6 ppm, respectively. Carrier positions for ^{15}N, ^{13}C, and ^1H were 117.4, 58.2, and 8.40 ppm, respectively. Spectra were acquired with 66 complex points in t_1, 150 complex points in t_2, and 24 scans per t_1/t_2 increment, resulting in a total experimental time of approximately 60 h. Details of the 3D multiple quantum HNCOCA experiment are described elsewhere (Brutscher et al., 1995). Spectral widths for ^{15}N, ^{13}C, and ^1H were 30, 40, and 6 ppm, respectively. Carrier positions for ^{15}N, ^{13}C, and ^1H were 121.8, 174.8 (phase shifted to 58.2 ppm for excitation of the C^α), and 8.40 ppm, respectively. Spectra were acquired with 41 complex points in t_1, 128 complex points in t_2, and 8 scans per t_1/t_2 increment, resulting in a total experimental time of approximately 35 h. For the ^{15}N-edited experiments, further solvent suppression was accomplished by light presaturation (approximately 10 Hz) during the relaxation delay of 1.2 s. The field strengths for WALTZ-16 decou-

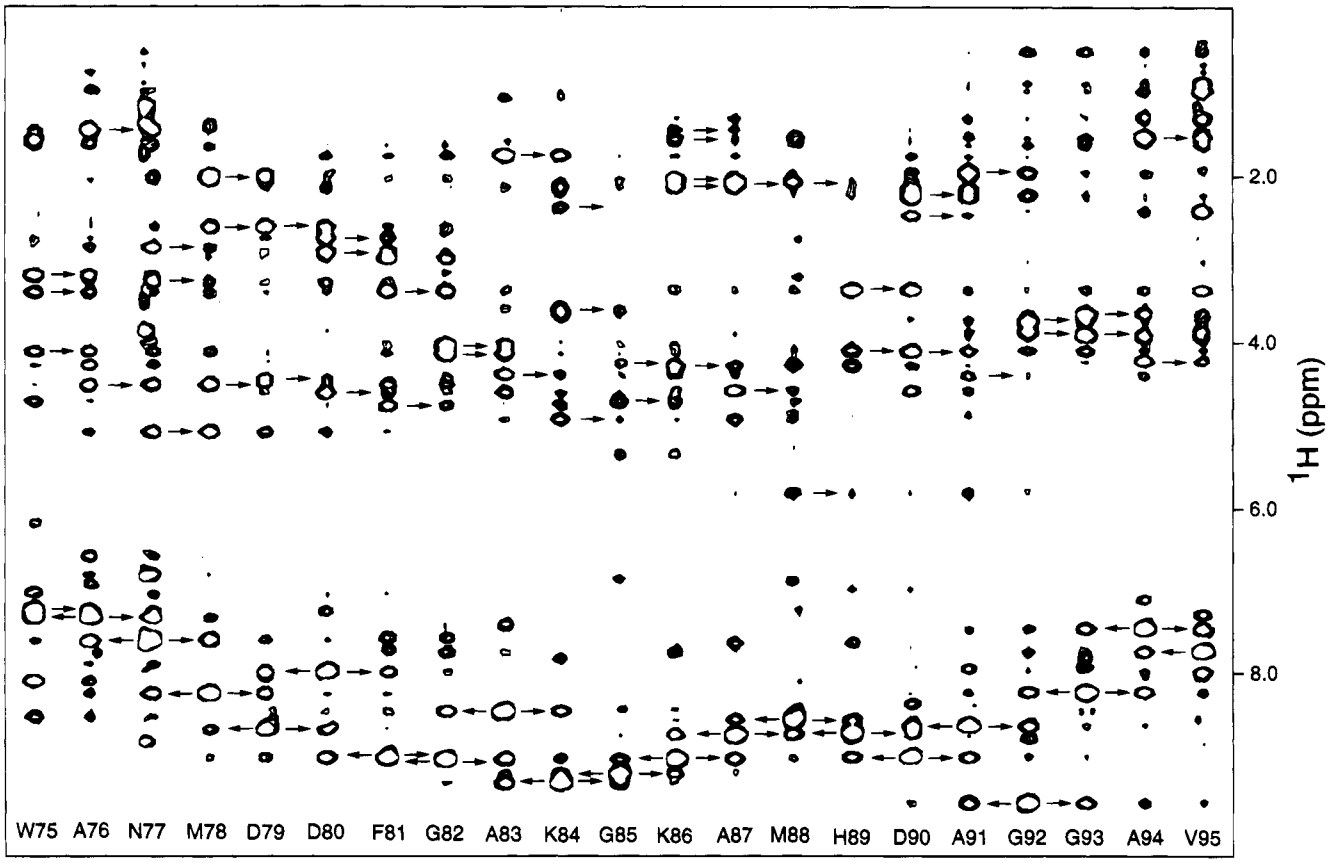

FIGURE 1: 2D representation of the NOESY-HSQC 3D experiment for the sequential assignment of W75−V95. The mixing time was 120 ms. Each residue is presented as a small region of the 2D spectrum taken at the ^{15}N frequency and centered at the H^N frequency (Table 1 of Supplementary Material). Arrows are drawn for interresidue NOEs. Note that the presence of $d_{NN(i,i+3)}$ connectivities suggests the onset of spin diffusion in the present experiment.

pling (Shaka et al., 1983) of ^{1}H and ^{15}N were 2.8 and 2.1 kHz, respectively. Quadrature detection in the indirectly-detected dimensions was obtained by the TPPI-States method (Marion et al., 1989a).

All data were processed using the FELIX program version 2.1 (Biosym Technologies). The indirect dimensions of 2D data sets were multiplied by a skewed sine bell function and zero-filled to result in 2048 × 1024 matrices. For ^{15}N-edited 3D data sets, the number of data points in the ^{15}N dimension was increased 25% by linear prediction (Olejniczak & Eaton, 1990). In addition, the indirect ^{1}H dimensions of the TOCSY-HSQC and NOESY-HSQC 3D experiments were increased 25% by linear prediction. The resulting data were multiplied by a skewed sine bell function and zero-filled. Final 3D matrices were 512 × 128 × 256, 512 × 128 × 256, 512 × 128 × 128, 512 × 128 × 64, 512 × 128 × 256, and 512 × 128 × 256 real points for the TOCSY-HSQC, NOESY-HSQC, HSQC-NOESY-HSQC, HNHA, HNCA, and HNCOCA experiments, respectively. For convenient analysis of 3D data sets, 2D equivalents were generated as previously described (Caffrey et al., 1994).

RESULTS AND DISCUSSION

Spin System Identification. The majority of the spin systems of *Rb. capsulatus* ferricytochrome *c′* could be identified by the TOCSY-HSQC 3D experiment, in which $^1H^N-^{15}N$ pairs are correlated to intraresidue ^{1}H (Marion et al., 1989b). The observation of single sets of correlations for each residue indicates that the *Rb. capsulatus* cytochrome *c′* complex is a symmetric dimer, as previously observed for the X-ray structures of the cytochromes *c′* from *Rps. molischianum*, *Rps. rubrum*, and *C. vinosum*, although the presence of nonsymmetric subunits in fast exchange cannot be ruled out. In total, intraresidue H^N-H^α correlations were observed in the TOCSY-HSQC 3D experiment for 105 of the 126 amino acids (129 residues minus 3 prolines). Moreover, the H^α for 104 of the 126 residues could be unambiguously assigned by the HNHA 3D experiment (Vuister & Bax, 1993), which uniquely correlates the H^N-H^α and is thus useful in the H^α assignment as well as for the determination of $^3J_{HN\alpha}$ coupling constants (discussed below). The missing residues in the TOCSY-HSQC and HNHA experiments are presumably due to increased relaxation rates of the H^N, H^α, or ^{15}N nuclei that are in closest contact with the unpaired electrons of the paramagnetic center. Nonetheless, the relatively high quality of the TOCSY data can be attributed to the 8 mM protein concentration, which significantly increases the signal to noise ratios. Unfortunately, further increases in protein concentration were not possible due to protein aggregation, as evidenced by the increased line widths that were observed for protein concentrations greater than 8 mM.

Sequential Assignment. The majority of the ^{1}H and ^{15}N resonances of *Rb. capsulatus* ferricytochrome *c′* could be sequentially assigned by the NOESY-HSQC 3D experiment, in which $^1H^N-^{15}N$ pairs are correlated to intra- and interresidue ^{1}H (Marion et al., 1989b). Examples of the assignments for residues W75−V95 are given in Figure 1, which

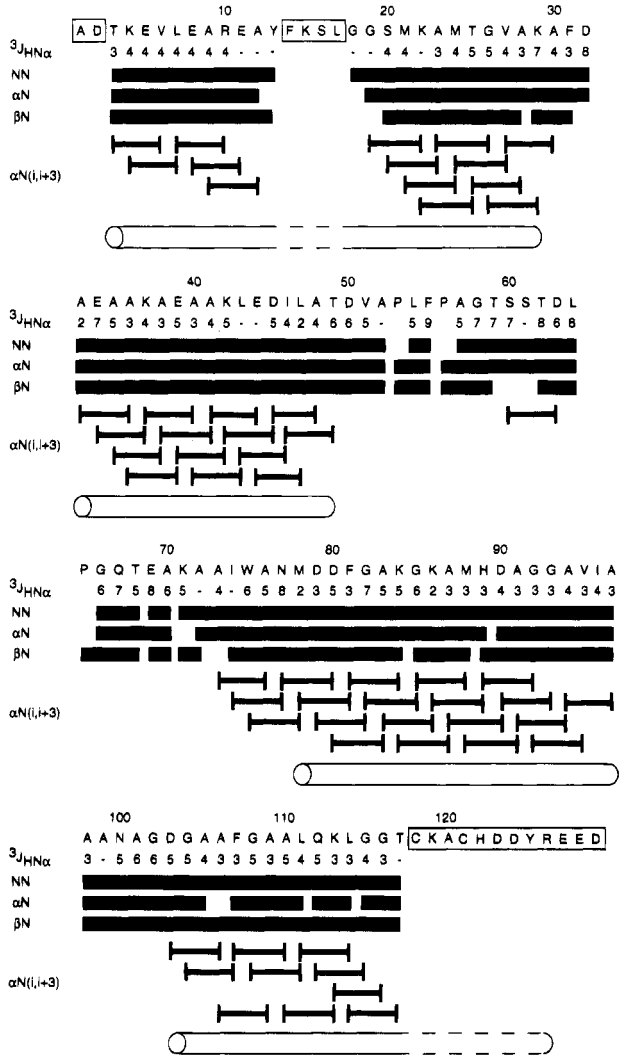

FIGURE 2: Schematic summary of the sequential connectivities for the assignment of *Rb. capsulatus* ferricytochrome *c'*. No distinctions are made for relative intensities. Unassigned residues are boxed. The $^3J_{HN\alpha}$ coupling constants are listed in units of Hz and accurate to ±1 Hz. The helical regions identified by the $d_{\alpha N(i,i+3)}$ and $^3J_{HN\alpha}$ coupling constants are shown by solid lines. The dotted lines for helices 1 and 4 represent helical structure based on expected homologies with known X-ray structures.

presents 2D representations of the 3D data set. In this figure, each residue is represented by a small region of the 2D plane at a given ^{15}N frequency and centered at a given $^1H^N$ frequency. Short-range $d_{NN(i,i+1)}$, $d_{\alpha N(i,i+1)}$, and $d_{\beta N(i,i+1)}$ connectivities are shown by horizontal lines. For example, N77 is shown to precede M78 by the characteristic $d_{NN(i,i+1)}$, $d_{\alpha N(i,i+1)}$, and $d_{\beta N(i,i+1)}$ connectivities. In many cases, the presence of $d_{NN(i,i+2)}$, $d_{\alpha N(i,i+2)}$, and $d_{\beta N(i,i+2)}$ connectivities aids the assignment. Moreover, $d_{\alpha N(i,i+3)}$ connectivities, characteristic of helical regions, are clearly observed for many of the residues (e.g., M88). In cases where the H^N of consecutive residues were degenerate (e.g., L7−E8 and G26−V27), the HSQC-NOESY-HSQC experiment was especially useful for establishing connectivity (data not shown). A summary of the short-range and medium-range connectivity patterns is given in Figure 2. In this figure, no distinction for the relative intensities of the NOEs is presented because it presupposes uniform relaxation effects within the molecule. As discussed in the introduction, the paramagnetic effect on nuclear relaxation exhibits a $1/r^6$ distance dependency; thus, uniform relaxation is clearly not the case in paramagnetic macromolecules. Consequently, we prefer to make no distinction for NOE intensities at the present level of examination. In total, backbone ^1H and ^{15}N have been assigned for 108 of the 126 residues present in *Rb. capsulatus* cytochrome *c'*, which represents 86% of the total. The significance of the unassigned residues, which are boxed in Figure 2, will be discussed below.

Assignment of Backbone ^{13}C. At a late stage in the assignment process, a small amount of *Rb. capsulatus* cytochrome *c'* labeled with ^{13}C and ^{15}N became available. Using the HNCA and multiple-quantum HNCOCA 3D experiments performed on a 0.5 mM sample, the majority of backbone ^{13}C could be assigned on the basis of the ^1H and ^{15}N assignments described above. The multiple-quantum HNCOCA experiment was especially useful to correlate $^1H-^{15}N$ pairs to CO_{i-1} and C^α_{i-1} due to its high sensitivity and resolution properties (Brutscher et al., 1995). In Figure 3, an example of the quality of the HNCOCA 3D experiment is given for the backbone ^{13}C assignment of N100−G115. The ^{13}C assignments are useful in several respects. First, the HNCA and HNCOCA experiments are complementary because they correlate $^1H_i-^{15}N_i$ pairs with their $^{13}C^\alpha_i$ and $^{13}C^\alpha_{i-1}$ resonances, respectively. Thus, the experiments provide independent confirmation of the sequential assignment that was originally based on NOE. Second, the $^{13}C^\alpha$ chemical shifts are characteristic of amino acid type (Richarz & Wüthrich, 1978) and thus provide an independent check of the assignment for a given residue. Finally, the perturbations of ^{13}CO and $^{13}C^\alpha$ chemical shifts from their random coil values can be used to identify secondary structures in proteins (to be discussed below).

Secondary Structure. In NMR studies of proteins, helices are characterized by the presence of $d_{\alpha N(i,i+3)}$ connectivities and $^3J_{HN\alpha}$ coupling constants that are less than 6 Hz (Wüthrich, 1986). A summary of the $d_{\alpha N(i,i+3)}$ connectivities that were observed in the NOESY-HSQC 3D experiment is presented in Figure 2. In addition, the $^3J_{HN\alpha}$ coupling constants, which were calculated from the relative intensities of the H^N-H^α cross peaks and the diagonal peaks in the HNHA 3D experiment (Vuister & Bax, 1993), are presented. Together the $d_{\alpha N(i,i+3)}$ connectivities and $^3J_{HN\alpha}$ coupling constants suggest that there are four helical regions in *Rb. capsulatus* ferricytochrome *c'*: residues 3−29, 33−49, 78−97, and 103−117. The justification for considering residues 3−29 as one continuous helix will be discussed below.

$^1H^\alpha$, $^{13}C^\alpha$, and ^{13}CO chemical shifts are additional indicators of secondary structure in proteins [for a review, see Wishart and Richards (1991)]. In paramagnetic heme proteins, chemical shifts are also affected by the ring current effects of the heme and the unpaired electrons of the iron (Wüthrich, 1976). Previously, we demonstrated that ring current effects in heme proteins did not diminish the information content of $^{13}C^\alpha$ and ^{13}CO chemical shifts, in contrast to $^1H^\alpha$ chemical shifts (Caffrey et al., 1994). In Figure 4, the secondary chemical shifts for the $^1H^\alpha$, $^{13}C^\alpha$, and ^{13}CO of *Rb. capsulatus* ferricytochrome *c'* are shown. Helical regions identified by the $d_{\alpha N(i,i+3)}$ connectivities, and $^3J_{HN\alpha}$ coupling constants are denoted by cylinders. In general, the secondary shifts of the $^{13}C^\alpha$ and ^{13}CO, which are shifted downfield from their random coil values in helices, correspond very well to the secondary structure derived by NOEs and coupling constants. Exceptions occur

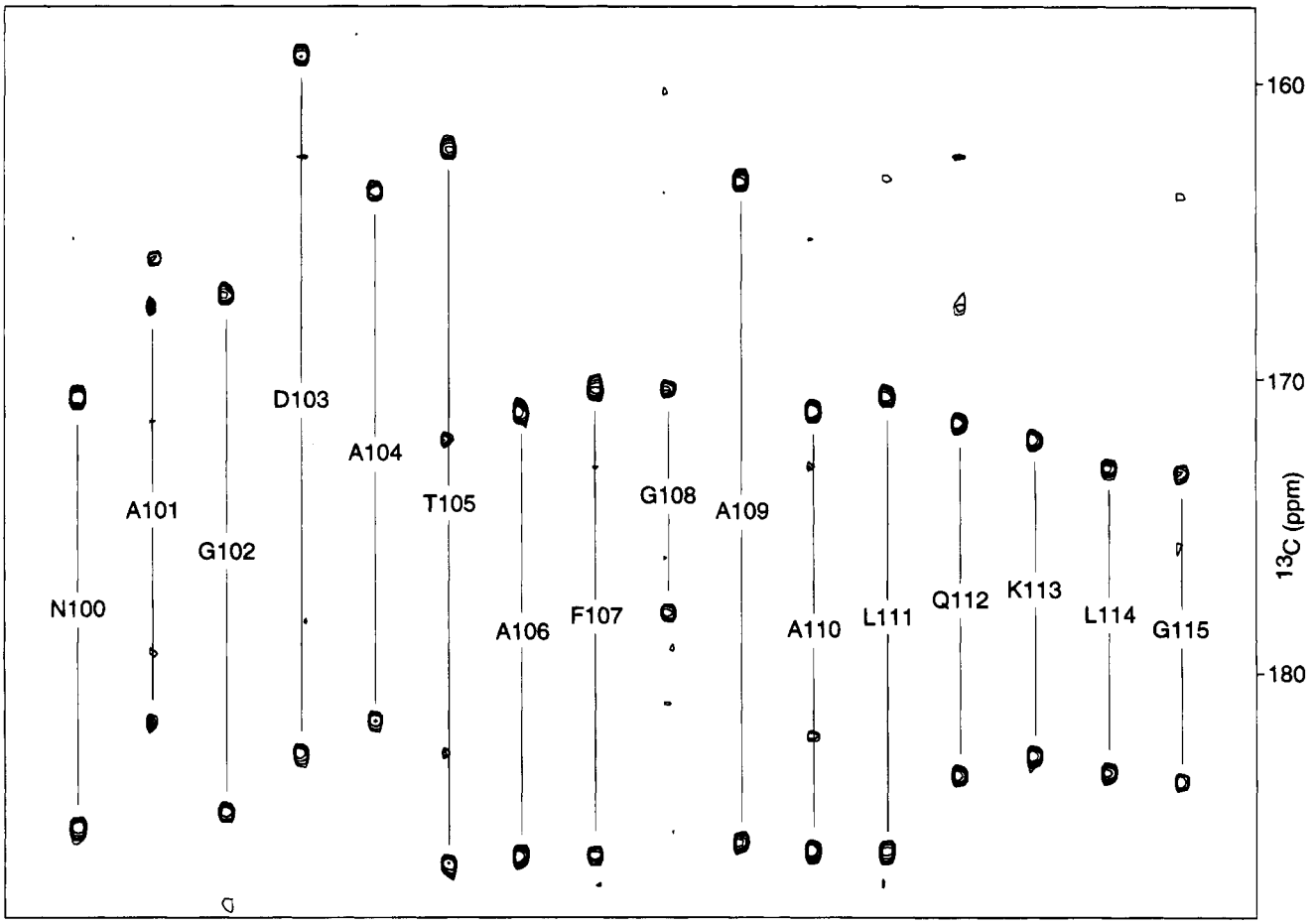

FIGURE 3: 2D representation of the HNCOCA 3D experiment for the sequential assignment of N100−G115. Each residue is presented as a small region of the 2D spectrum taken at the ^{15}N frequency and centered at the H^N frequency (Table 1 of Supplementary Material). The $^{13}CO_{i-1}$ frequency is given by the midpoint of the two peaks, and the $^{13}C^{\alpha}_{i-1}$ frequency is given by the distance between each of the peaks and the midpoint [cf. Simorre et al. (1994) and Brutscher et al. (1994) for discussions of multiple-quantum experiments].

for the residues flanking the unassigned region comprising of residues 14−17. As will be discussed below, these residues are in closest proximity to the heme iron and thus are expected to experience the largest effects of paramagnetism on chemical shifts. However, a break in helix-1 cannot be ruled out by the present set of NMR data. Nonetheless, the $^{13}C^{\alpha}$ and ^{13}CO chemical shifts are clearly useful indicators of secondary structure, even in paramagnetic heme proteins. In contrast, $^{1}H^{\alpha}$ chemical shifts are a less reliable indicator of secondary structure in paramagnetic heme proteins.

It is of interest to compare the *Rb. capsulatus* cytochrome *c′* secondary structure to the cytochromes *c′* for which X-ray structures exist. In Figure 5, the amino acid sequences have been aligned for the cytochromes *c′* from *Rb. capsulatus*, *C. vinosum*, *Rps. molischianum*, and *Rps. rubrum*. As previously noted by Meyer and Kamen (1982), the cytochromes *c′* exhibit a relatively low conservation of amino acid sequence (with the exception of the heme binding region). Specifically, the *Rb. capsulatus* cytochrome *c′* exhibits 24%, 22%, and 36% amino acid identity to the cytochromes *c′* from *C. vinosum*, *Rps. molischianum*, and *Rps. rubrum*, respectively. In Figure 5, the shaded regions of the amino acid sequences signify helical regions that have been derived by either NMR spectroscopy (*Rb. capsulatus* cytochrome *c′*) or X-ray crystallography (*C. vinosum*, *Rps. molischianum*, and *Rps. rubrum* cytochromes *c′*). As shown in Figure 2, helix-1 of *Rb. capsulatus* cytochrome *c′* is interrupted by the inability to assign residues 14−17. Nonetheless, the conservation of helix-1 between the X-ray structures of the cytochromes *c′* and the absence of proline residues in this region suggest that helix-1 of *Rb. capsulatus* cytochrome *c′* is continuous. Moreover, long-range NOEs between the two parts of helix-1 and helices-2 and -4 are consistent with this interpretation (discussed below). Thus, helix-1 of *Rb. capsulatus* cytochrome *c′* appears to be homologous to the other cytochromes *c′*. Helix-2 is clearly most similar to the *C. vinosum* and *Rps. rubrum* cytochromes *c′*, which exhibit a helix that is shifted and shortened with respect to the *Rps. molischianum* cytochrome *c′*. Helix-3 of *Rb. capsulatus* cytochrome *c′* possesses a C-termination point that is most similar to the *C. vinosum* and *Rps. rubrum* cytochromes *c′*. Helix-4 of *Rb. capsulatus* cytochrome *c′* appears to be homologous to the other cytochromes *c′*; however, the inability to assign eight residues at the carboxy terminus of the helix leaves some ambiguity for the termination site of helix-4. In conclusion, *Rb. capsulatus* cytochrome *c′* exhibits a secondary structure that is most similar to the *C. vinosum* and *Rps. rubrum* cytochromes *c′*.

Assignment of Aromatic Side Chains. The spin systems of F31, F55, F81, and F107 are clearly visible in the TOCSY 2D experiment. The phenylalanine spin systems were unambiguously assigned by the observation of NOEs between C2,6H and previously assigned H^{α} and H^{β} in the NOESY 2D experiment. The spin system of W75 was also clearly visible in the TOCSY 2D experiment and was unambiguously assigned by NOEs between the C2H and

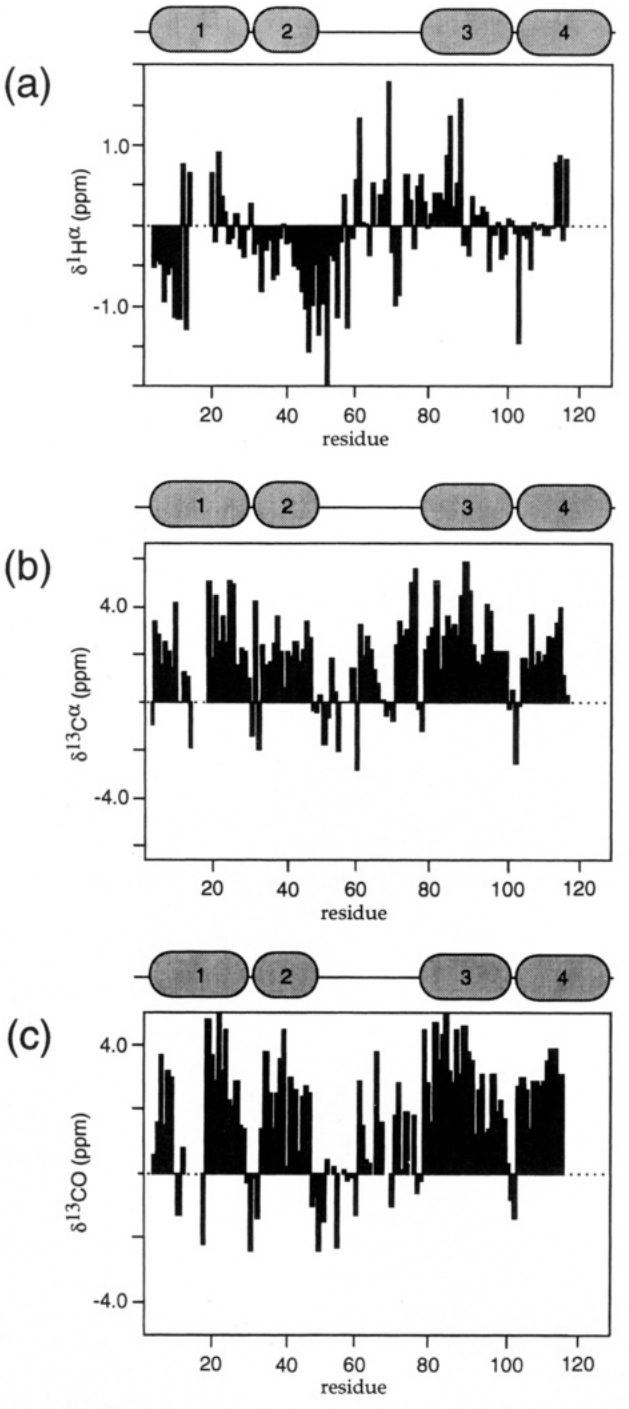

FIGURE 4: Secondary chemical shifts for *Rb. capsulatus* ferricytochrome *c′* (a) $^1H^\alpha$, (b) $^{13}C^\alpha$, and (c) ^{13}CO. Secondary chemical shifts are calculated as $\Delta\delta = \delta_{obs} - \delta_{rc}$, where δ_{obs} are the observed values and δ_{rc} are the random coil values for $^1H^\alpha$ (Wüthrich, 1986) or backbone ^{13}C (Richarz & Wüthrich, 1978). Unassigned residues are indicated by dotted lines. Helical regions are indicated by cylinders.

previously assigned H^β in the NOESY 2D experiment. Note that the NOESY 2D experiment utilized a heteronuclear half-filter to select for ^1H not bound to ^{15}N and thus simplifies the NOESY spectra by filtering out the H^N resonances. The C2H and C4H of H89 were assigned by their intra, and interresidue NOEs to backbone H^N in the NOESY-HSQC 3D experiment. In contrast, the spin systems for Y13, F14, H122, and Y125 were not apparent in the TOCSY or NOESY 2D experiments. Not unexpectedly, the missing aromatic ^1H correspond to residues for which the backbone ^1H and ^{15}N could not be assigned. This observation is consistent with their close proximity to the paramagnetic center because their observation is expected to be prohibited by relatively fast relaxation rates (discussed below).

Assignment of Side Chain ^{15}NH. The side chain ^{15}NH of Q67, W75, N77, N100, and Q112 was identified by the TOCSY-HSQC 3D experiment and assigned by the NOESY-HSQC 3D experiment. Specifically, the side chain ^{15}NH of W75 was assigned by NOEs between the ^{15}NH and the previously assigned C2H and C7H. The side chain ^{15}NHs of N77 and Q100 were assigned by NOEs between the ^{15}NH and the previously assigned H^α and H^β. The side chain ^{15}NHs of Q67 and Q112 were assigned by NOEs between the ^{15}NH and the previously assigned H^β and H^δ. In contrast, the side chain ^{15}NHs of R10, H89, H122, and R125 were not apparent in the HSQC 2D experiment or TOCSY-HSQC and NOESY-HSQC 3D experiments. In the case of H122 and R125, the missing ^{15}NH correspond to residues for which the backbone ^1H and ^{15}N could not be assigned, and hence the side chain ^{15}NHs are expected to be difficult to observe for the reasons discussed above.

Topological Model. A topological model of *Rb. capsulatus* ferricytochrome *c′* can be constructed on the basis of the observed secondary structure and long-range intrasubunit NOEs. In Figure 6, a contact plot is presented for medium- and long-range NOEs that could be identified in the filtered NOESY 2D experiment and the NOESY-HSQC 3D experiment. Figure 6 shows that there are extensive contacts between helix-1 (residues 3−29) and helix-2 (residues 33−49). Helix-2 exhibits extensive contacts with helix-3 (residues 78−97). Helix-3 exhibits contacts with helix-4 (residues 103−117). Moreover, helix 1 shows contacts to helix 4. Note that the antidiagonal nature of the interhelical contacts is consistent with an antiparallel orientation between consecutive helices. The contacts between the helices can only be interpreted by the topological model presented in Figure 7. As shown by Figure 7, NOEs between helices-1 and -3 are expected to be weaker due to the increased distance between the helices. The NMR data clearly establish that the *Rb. capsulatus* ferricytochrome *c′* is a four-helix bundle protein that is structurally homologous to the cytochromes *c′*, for which X-ray structures exist (i.e., cytochromes *c′* from *C. vinosum*, *Rps. molischianum*, and *Rps. rubrum*). Interestingly, very few intersubunit NOEs could be unambiguously identified. Analysis of the X-ray crystal structures of *C. vinosum*, *Rps. molischianum*, and *Rps. rubrum* cytochromes *c′* shows that most of the intersubunit contacts are hydrophobic in nature and occur between helices-1 and -2. The absence of assignments for residues 14−17, which are at the interface of the two subunits, results in the absence of observable NOEs in this region. Furthermore, the X-ray structures suggest that most of the contacts occur between sidechains. Due to a large amount of spectral overlap, the present NOE analysis has relied heavily on ^{15}N-edited experiments, for which side chain−side chain NOEs are absent. The ^{13}C-labeled sample might be useful for the observation of side chain−side chain NOEs; however, the small concentration presently available limits the sensitivity of NOE experiments. Thus, it appears that characterization of the contact region between subunits awaits the application of genetic techniques to clone and overexpress the *Rb. capsulatus* cytochrome *c′*, as previously applied to *Rb. capsulatus* cytochrome c_2 (Caffrey et al., 1992).

```
          1                   10                  20
RC: - - A D T K E V L E A R E A Y F K S L G G S M K A M T G V A K - -
CV: A G L S P E E Q I E T R Q A G Y E F M G W N M G K I K A N L E G -
RM: Q Q S K P E D L L K L R Q G L M Q T L K S Q W V P I A G F A A G K
RR: - - A D P A A Y V E Y R K S V L S A T S N Y M K A I G I T L K E -

          30                  40                  50                  60
RC: A F D A E A A K A E A A K L E D I L A T D V A P L F P A G T S S T
CV: E Y N A A Q V E A A A N V I A A I A N S G M G A L Y G P G T D K N
RM: A D L P A D A A Q R A E N M A M V A K L - A P I G W A K G T E A L
RR: D L A V P N Q T A D H A K A I A S I M E T L P A A F P E G T A G I

                    70                  80                  90
RC: D L P G Q T E A K A A I W A - N M D D F G A K G K A M H D A G G A
CV: V G D V K T R V K P E F F Q - N M E D V G K I A R E F V G A A N T
RM: P - - - N G E T K P E A F G S K S A E F L E G W K A L A T E S T K
RR: A - - - K T E A K A A I W K - D F E A F K V A S K K S Q D A A L E

          100                 110                 120
RC: V I A A A N A G D G A A F G A A L Q K L G G T C K A C H D D Y R E E D
CV: L A E V A A T G E A E A V K T A F G D V G A A C K S C H E K Y R A K
RM: L A A A A K A G - P D A L K A Q A A A T G K V C K A C H E E F K Q E
RR: L A S A A E T G D K A A I G A K L Q A L G G T C K A C H K E F K A D
```

FIGURE 5: Amino acid sequence alignments for the cytochromes *c′* from *Rb. capsulatus* (RC), *C. vinosum* (CV), *Rps. molischianum* (RM), and *Rps. rubrum* (RR). Boxed residues correspond to amino acids that are conserved in at least three of the four species. Shaded regions correspond to helical regions of cytochromes *c′*, based on NMR spectroscopy (*Rb. capsulatus*, present study) or x-ray crystallography [*C. vinosum* (Ren et al., 1993); *Rps. molischianum* (Finzel et al., 1985); *Rps. rubrum* (Yasui et al., 1992)].

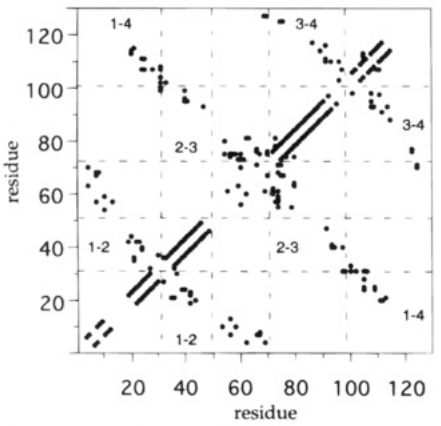

FIGURE 6: Cross-correlation map for medium and long-range NOEs ($i, i > 2$). Dotted lines are drawn at the N- and C-termination points of helices.

Unassigned Residues. Finally, it is of interest to discuss the backbone resonances that could not be assigned. The unassigned residues are found in three regions: residues 1−2, 14−17, and 118−129. In Figure 8, the Fe−N and Fe−H^N distances have been plotted for the X-ray structure of *C. vinosum* ferricytochrome *c′* (Ren et al., 1993). Based on amino acid sequence identity and secondary structure (Figures 2 and 5), the *Rb.capsulatus* cytochrome *c′* three-dimensional structure is expected to be most homologous to that of *Rps rubrum*; however, the *Rps. rubrum* cytochrome *c′* coordinates have not yet been deposited in the Brookhaven Protein Database. Consequently, we have chosen the *C. vinosum* cytochrome *c′* structure, which is more homologous to *Rb. capsulatus* than that from *Rps. molischianum*. Interestingly, the H^N and ^{15}N of residues 14−17 and 118−125 are in closest contact with the iron paramagnetic center For example, nuclei that are 9 Å from the paramagnetic center are expected to have paramagnetic relaxation rates that are more than 3 times faster than nuclei that are 11 Å from the paramagnetic center. As a consequence of this close contact, these residues exhibit signal to noise ratios that are decreased by a factor of 3 and hence are difficult to detect. Thus, the present set of experimental conditions appear to prohibit detection of nuclei that are less than approximately 9 Å from the iron. This leaves A1, D2, and D129, which are found at the termini of the polypeptide chain and may be absent from the NMR spectra due to motional averaging on an intermediate time scale.

Concluding Remarks. To our knowledge the present work represents the first extensive NMR assignment of a cytochrome *c′* and lays the foundation for future studies of the structural, dynamic, and ligand-binding properties of this interesting class of proteins. The success in assigning the resonances of a 28 kDa paramagnetic protein is undoubtedly due to the application of ^{15}N-edited NMR experiments to a concentrated protein solution. This suggests that in favorable cases of protein solubility, relatively large molecular weight complexes can be extensively assigned by ^{15}N-edited experiments. For example, the present result demonstrates the

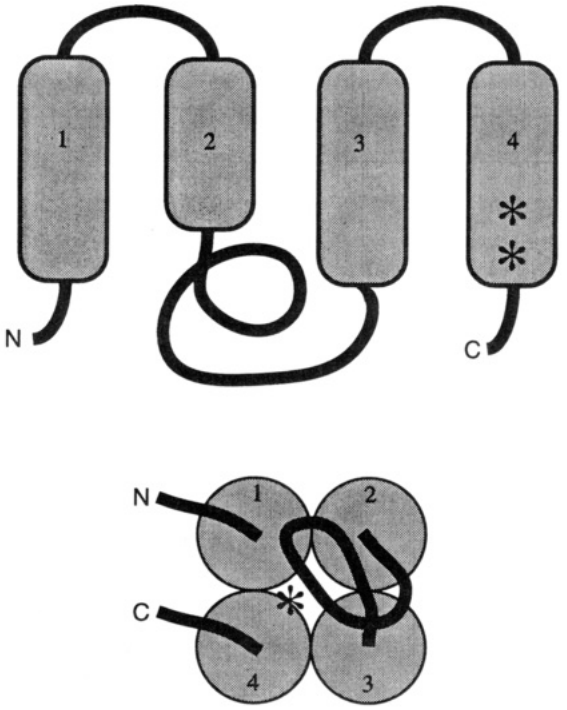

FIGURE 7: Topological model of the *Rb. capsulatus* ferricytochrome *c′* tertiary structure based on medium- and long-range NOEs. Asterisks represent the sites where the heme is covalently bonded to the peptide (i.e., C118 and C121).

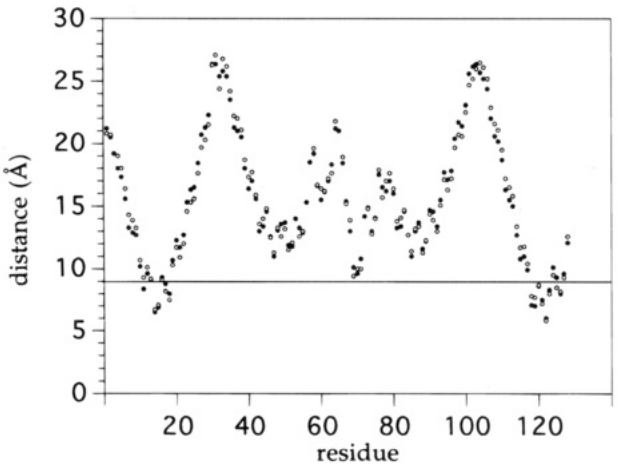

FIGURE 8: Fe−N (solid circles) and Fe−H^N (open circles) distances for *C. vinosum* ferricytochrome *c′* (Ren et al., 1993). Numbering corresponds to that of *Rb. capsulatus* cytochrome *c′*. For reference a solid line is drawn at a distance of 9 Å.

ability to assign a 28 kDa complex made up of identical 14 kDa subunits and uniformly labeled with ^{15}N. In addition, we have shown the value of assigning the backbone ^{13}C, using a less concentrated sample uniformly labeled with ^{13}C and ^{15}N. This latter approach may be interesting for cases where the cost of preparing a ^{13}C labeled sample was previously considered to be prohibitive. Finally, we note that calculation of the *Rb. capsulatus* ferricytochrome *c′* structure is a difficult undertaking due to the unobserved resonances which are presumably near the heme. Consequently, additional distance information will be required for a structure calculation. Possible approaches to overcome this problem include: (1) 1D and 2D NOE experiments that are optimized for the observation of fast relaxing nuclei by use of fast recycle times and short mixing times [cf., LaMar and Ropp (1993) and Satterlee et al. (1993)]; (2) augmentation of the current NOE data with relaxation data for individual nuclei, which reflect their distance to the iron center, in a manner similar to that recently proposed by the Fesik laboratory for diamagnetic proteins which are spin-labeled (Yu et al., 1994). Both approaches are currently under study in our laboratory.

ACKNOWLEDGMENT

We gratefully acknowledge amino acid sequence information provided by Professor R. Ambler (University of Edinburgh). This work was supported in part by the Commissariat à L'Energie Atomique (CEA), Centre National de la Recherche Scientifique (CNRS), Biosym Technologies. M. Caffrey gratefully acknowledges support by the Human Frontiers of Science Program and the CNRS. B. Brutscher is supported by a Bruker-CEA fellowship.

SUPPLEMENTARY MATERIAL AVAILABLE

One table containing the ^1H, ^{15}N, and ^{13}C chemical shift assignments for *Rb. capsulatus* ferricytochrome *c′* and one figure showing an example of the TOCSY-HSQC spectra for *Rb. capsulatus* ferricytochrome *c′* (4 pages). Ordering information is given on any current masthead page.

REFERENCES

Banci, L., Bertini, I., Turano, P., & Vicens Olivier, M. (1992) *Eur. J. Biochem. 204*, 107−112.
Bartsch, R. (1978) in *The Photosynthetic Bacteria* (Clayton, R., & Sistrom, W., Eds.) pp 249−280, Plenum, New York.
Bax, A., & Pochapsky, S. (1992) *J. Magn. Reson. 99*, 638−643.
Bodenhausen, G., & Ruben, D. (1980) *Chem. Phys. Lett. 69*, 185−189.
Brutscher, B., Simorre, J.-P., Caffrey, M., & Marion, D. (1994) *J. Magn. Reson. 105*, 77−82.
Brutscher, B., Cordier, F., Simorre, J.-P., Caffrey, M., & Marion, D. (1995) *J. Biomol. NMR 5*, 202−206.
Caffrey, M., Davidson, E., Cusanovich, M., & Daldal, F. (1992) *Arch. Biochem. Biophys. 292*, 419−426.
Caffrey, M., Brutscher, B., Simorre, J.-P., Fitch, J., Cusanovich, M., & Marion, D. (1994) *Eur. J. Biochem. 221*, 63−75.
Cusanovich, M., & Gibson, Q. (1973) *J. Biol. Chem. 248*, 822−834.
Davis, D., & Bax, A. (1985) *J. Am. Chem. Soc. 107*, 2820−2821.
Doyle, M., Weber, P., & Gill, S. (1985) *Biochemistry 24*, 1987−1991.
Doyle, M., Gill, S., & Cusanovich, M. (1986) *Biochemistry 25*, 2509−2516.
Finzel, B., Weber, P., Hardman, K., & Salemme, F. (1985) *J. Mol. Biol. 186*, 627−643.
Grzesiek, S., & Bax, A. (1992) *J. Magn. Reson. 96*, 432−440.
Ikura, M., Bax, A., Clore, G., & Gronenborn, A. (1990) *J. Am. Chem. Soc. 112*, 9020−9026.
Kassner, R. (1991) *Biochim. Biophys. Acta 1058*, 8−12.
Kay, L., Marion, D., & Bax, A. (1989) *J. Magn. Reson. 84*, 72−84.
La Mar, G., & Ropp, J. (1993) in *Biological Magnetic Resonance* (Berliner, L., & Reuben, J., Eds.) Vol. 12, pp 1−78, Plenum Press, New York.
La Mar, G., Jackson, T., Dugad, L., Cusanovich, M., & Bartsch, R. (1990) *J. Biol. Chem. 265*, 16173−16180.
Maltempo, M., & Moss, T. (1976) *Q. Rev. Biophys. 9*, 181−215.
Marion, D., Ikura, M., Tschudin, R., & Bax, A. (1989a) *J. Magn. Reson. 85*, 393−399.
Marion, D., Driscoll, P., Kay, L., Wingfield, P., Bax, A., Gronenborn, A., & Clore, G. (1989b) *Biochemistry 28*, 6150−6156.
Meyer, T., & Kamen, M. (1982) *Adv. Protein Chem. 35*, 105−212.

Monkara, F., Bingham, S., Kadir, F., McEwan, A., Thomson, A., Thurgood, A., & Moore, G. (1992) *Biochim. Biophys. Acta 1100*, 184−188.
Moore, G., & Pettigrew G. (1990) in *Cytochromes c: Evolutionary, Structural and Physiological Aspects*, Springer-Verlag, Berlin.
Olejniczak, E., & Eaton, H. (1990) *J. Magn. Reson. 87*, 628−632.
Otting, G., & Wüthrich, K. (1990) *Q. Rev. Biophys. 23*, 39−96.
Presnell, S., & Cohen, F. (1989) *Proc. Natl. Acad. Sci. U.S.A. 86*, 6592−6596.
Ren, Z., Meyer, T., & McRee, D. (1993) *J. Mol. Biol. 234*, 433−445.
Richarz, R., & Wüthrich, K. (1978) *Biopolymers 17*, 2133−2141.
Satterlee, J., Alam, S., Yi, Q., Erman, J., Constantinidis, I., Russell, D., & Moench, S. (1993) in *Biological Magnetic Resonance* (Berliner, L., & Reuben, J., Eds.) Vol. 12, pp 275−298, Plenum Press, New York.
Shaka, A., Keeler, J., Frenkiel, T., & Freeman, R. (1983) *J. Magn. Reson. 52*, 335−338.
Simorre, J.-P., Brutscher, B., Caffrey, M., & Marion, D. (1994) *J. Biomol. NMR 4*, 325−333.
Sklenàr, V., Piotto, M., Leppik, R., & Saudek V. (1993) *J. Magn. Reson. 102*, 241−245.
Swift, T. (1973) in *NMR of Paramagnetic Molecules*, Academic Press, New York.
Vuister, G., & Bax, A. (1993) *J. Am. Chem. Soc. 115*, 7772−7777.
Weaver, P., Wall, J., & Gest, H. (1975) *Arch. Microbiol. 105*, 207−216.
Wishart, D., Sykes, B., & Richards, F. (1991) *J. Mol. Biol. 222*, 311−333.
Wüthrich, K. (1976) in *NMR of Biological Research,* North Holland, Amsterdam.
Wüthrich, K. (1986) in *NMR of Proteins and Nucleic Acids*, John Wiley & Sons, New York.
Yasui, M., Harada, S., Kai, Y., Kasai, N., Kusunoki, M., & Matsuura, N. (1992) *J. Biochem. (Tokyo) 111*, 317−324.
Yu, L., Meadows, R., Wagner, R., & Fesik, S. (1994) *J. Magn. Reson. 104*, 77−80.

BI942905T